Article:
Georgiou, K., Jayaprakash, R. orcid.org/0000-0002-2021-1601 and Lidzey, D.G. orcid.org/0000-0002-8558-1160 (2020) Strong coupling of organic dyes located at the surface of a dielectric slab microcavity. The Journal of Physical Chemistry Letters, 11 (22). pp. 9893-9900. ISSN 1948-7185

https://doi.org/10.1021/acs.jpclett.0c02751

SUPPORTING INFORMATION

Strong Coupling of Organic Dyes Located at the Surface of a Dielectric Slab Microcavity

K. Georgiou[1]*, R. Jayaprakash and D.G. Lidzey*

Department of Physics and Astronomy, University of Sheffield, Hicks Building, Hounsfield Road, Sheffield S3 7RH, United Kingdom

* email: k.georgiou@sheffield.ac.uk , d.g.lidzey@sheffield.ac.uk

Table of Contents

[1] Current Address: Department of Physics, University of Cyprus, P. O. Box 20537, Nicosia 1678, Cyprus

1. Experimental Methods

Sample fabrication. To fabricate slab resonators, a Nb_2O_5 film of thickness between 100 and 200 nm was evaporated on to a quartz-coated glass substrate followed by a thicker SiO_2 layer having a thickness of 1.0 to 2.3 μm. Both layers were deposited at a deposition rate of 2 Å s^{-1} using an Ångstrom Engineering electron-beam evaporator held at a base pressure of 4 x 10^{-6} mbar. An organic semiconductor layer having a thickness of 100 to 250 nm was then deposited onto the SiO_2 layer by spin coating. The thickness of the organic layer was tuned by changing the speed of the spin coater, with its thickness measured using a Bruker Dektak XT profilometer. For strong coupling experiments of NK-2707, the two structures used consisted of 100 / 1000 / 100 nm and 200 / 2300 / 250 nm of Nb_2O_5 / SiO_2 / NK-2707 respectively. The structure used for the gas 'sensor' experiments as well as strong coupling in water consisted of 150 / 1700 / 225 nm of Nb_2O_5 / SiO_2 / MTPP respectively.

Organic molecule solutions. NK-2707 (supplied by Hayashibara Biochemical) was dissolved at 5% by mass in a solution of DI water and gelatine (20 mg mL^{-1}). NK-2707 / gelatine films were spin-coated using 100 μL of solution held at a temperature of 65°C. MTPP (supplied by Sigma-Aldrich) was dissolved at 10% by mass in a solution of PS (Mw = 192,000) in DCM (25 mg mL^{-1}). MTPP / PS films were spin-coated using 100 μL of solution at room temperature.

Angle-resolved white light optical reflectivity. Angular white light optical reflectivity measurements were performed using a goniometer setup, with light coupled to and from the goniometer using optical fibres. Two arms were mounted onto a common rotation stage allowing control over the angle of incidence and reflection. A fibre coupled Ocean Optics Halogen-Deuterium white light source (DH-2000-BAL) was mounted to the excitation arm and used to illuminate the sample. Reflected light was collected through an optical fibre mounted on the collection arm and directed into an Andor Shamrock SR-303i-A triple-grating imaging spectrograph with a focal length of 0.303 m.

Gas 'sensor' experiments. The samples were placed in a sealed chamber, with the containing either HCl and NH_3 gas. Samples were left in this chamber for a range of exposure times, after which they were removed into air and measured under ambient conditions using the goniometer optical-reflectivity setup, with each measurement taking around 100 seconds. The samples were then returned to the gas-exposure sample-chamber for further exposure and then re-measured. At present, we cannot exclude that small changes in the optical properties of molecules may occur during the course of the measurement under ambient conditions (i.e. in the absence of the HCl or NH_3 gas), however we believe that such changes (if they occur) are likely to relatively small and do not substantially change the outcome of the experiment. For experiments shown in Figure 3 the concentration of HCl and NH_3 in water was 33% and 25% by wt. respectively. Experiments shown in Figure 4a were performed using HCl that was diluted in water at a concentration of 25% by wt.

Strong coupling in water. The slab cavity was placed into a water-containing cuvette with the cuvette being sufficiently large that the structure was surrounded by water on all sides. The cuvette was placed onto a goniometer with white light angular reflectivity measured at angles of incidence and reflection (in water) between 7.5° and 29°.

Transfer matrix reflectivity model. A transfer matrix model (described in detail in the 'Basics of Optics of Multilayer Systems'[1]) has been used to calculate the angle-resolved reflectivity of the dielectric slab resonators. Here, the absorption of the different organic active layers was fitted using one or more Lorentz functions and used as input to the TMR model. By applying suitable scaling factors, this was then used to simulate the excitonic response of the various materials studied.

2. Cross section of reflectivity maps in empty microcavities

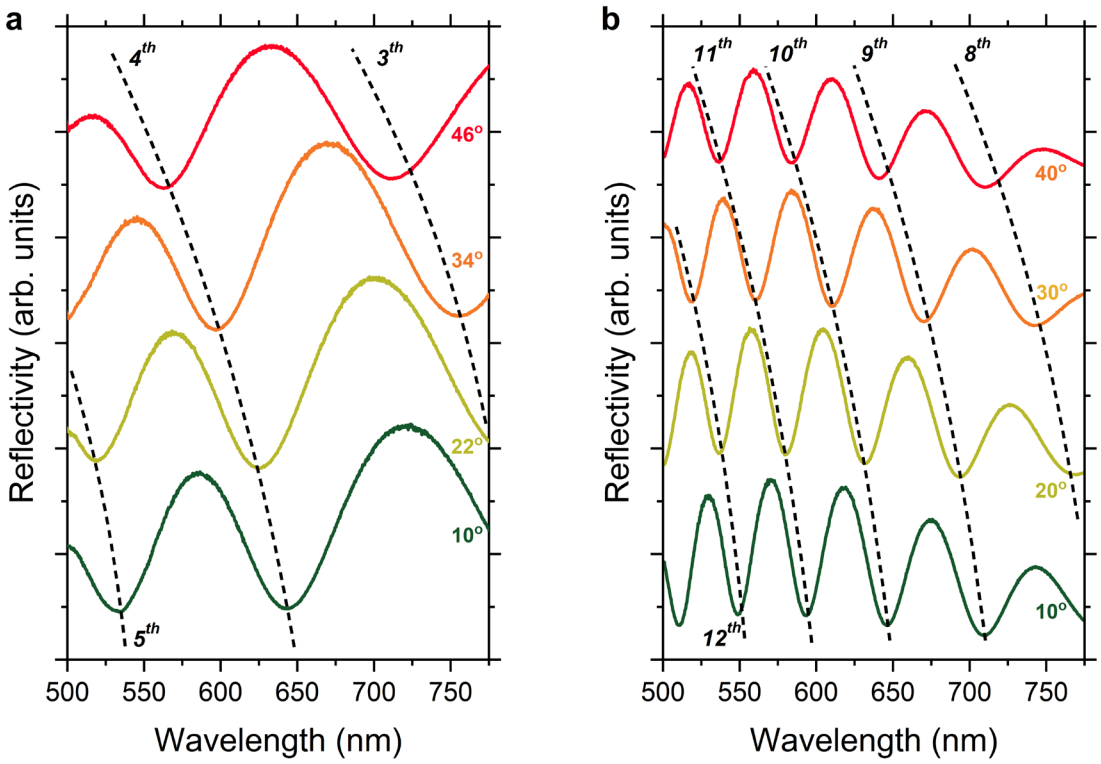

Figure S1. Angle-resolved cross sections of reflectivity maps. The plot shows white light reflectivity measured at four individual angles for a microcavity consisting of (a) 100 / 1000 nm thick layers of Nb_2O_5 / SiO_2 and (b) 200 / 2300 nm thick layers of Nb_2O_5 / SiO_2. The black dashed lines are guides to the eye that follow the dispersion of the confined optical modes.

3. Cross section of reflectivity maps in NK-2707 microcavities

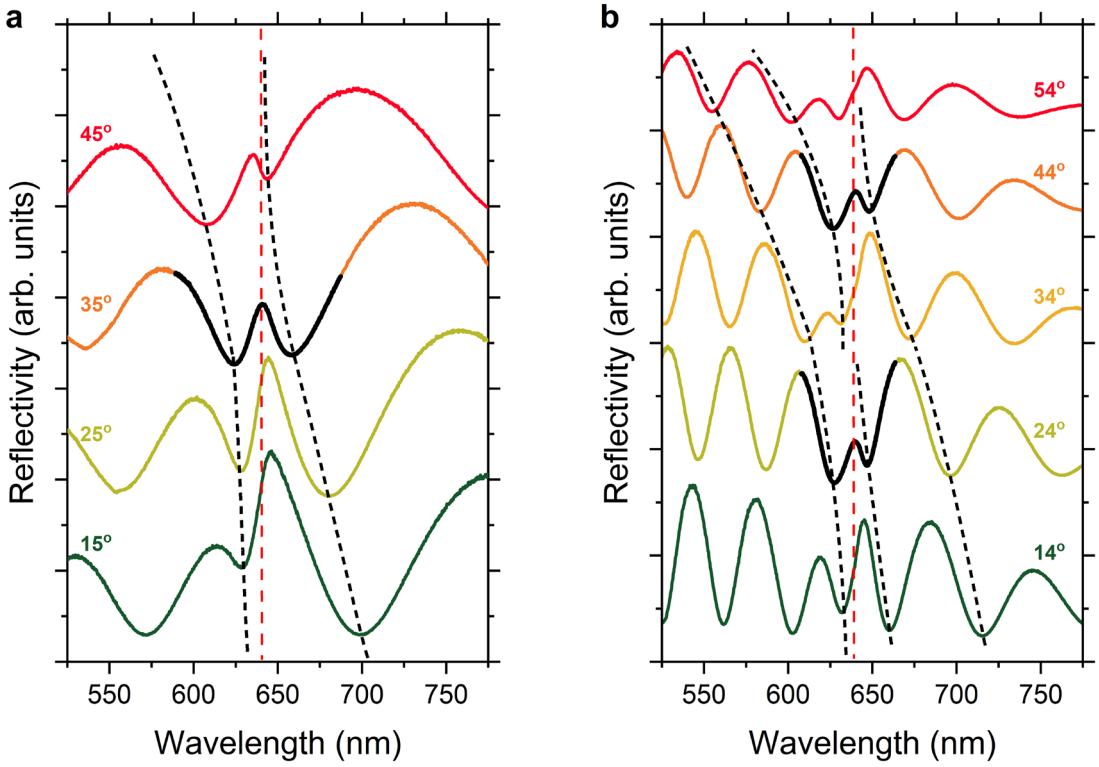

Figure S2. Angle-resolved cross sections of reflectivity maps. The plot shows measured white light reflectivity at (a) four individual angles for a microcavity consisting of 100 / 1000 / 100 nm thick layers of Nb_2O_5 / SiO_2 / NK-2707 and (b) at five individual angles of a microcavity consisting of 200 / 2300 / 250 nm thick layers of Nb_2O_5 / SiO_2 / NK-2707. The red dashed line marks the NK-2707 exciton around 638 nm. The black dashed lines are guides to the eye following the polariton dispersion and the black solid lines mark the energy splitting close to resonance.

4. Simulated strong-coupling in different Fabry-Perot resonator types

We have performed a series of TMR modelling experiments based on a structure composed of a typical J-aggregate dye film placed within a series of different microcavities, including those based on (i) two silver mirrors, (ii) a Distributed Bragg Reflector (DBR) and a silver mirror and (iii) two DBR-DBR mirrors. The results of these simulations are summarised in Table S1 showing calculated cavity Q-factor and the Rabi splitting energy.

Type of Resonator	Organic layer thickness nm	Rabi splitting energy meV	Microcavity Q-Factor
Ag-Ag	**350**	**188**	**69**
Ag-DBR	**350**	**133**	**282**
DBR-DBR	**250**	**92**	**634**
Dielectric Slab	**350**	**80**	**31**

Table S1. Values extracted from a TMR model for simulated strong coupling in Ag-Ag, Ag-DBR, DBR-DBR and Dielectric Slab Resonators.

To further highlight the effect of using a dielectric slab geometry in comparison to other types of microcavity architecture, the plot below shows reflectivity data recorded using typical J-aggregate films placed in strong-coupled cavities composed of Ag-Ag[2], Ag-DBR[3] and DBR-DBR[4] mirrors, along with data re-plotted from Figure S3. Here, data plotted using Ag-Ag, Ag-DBR and DBR-DBR mirrors has been taken from our previous papers[2–4].

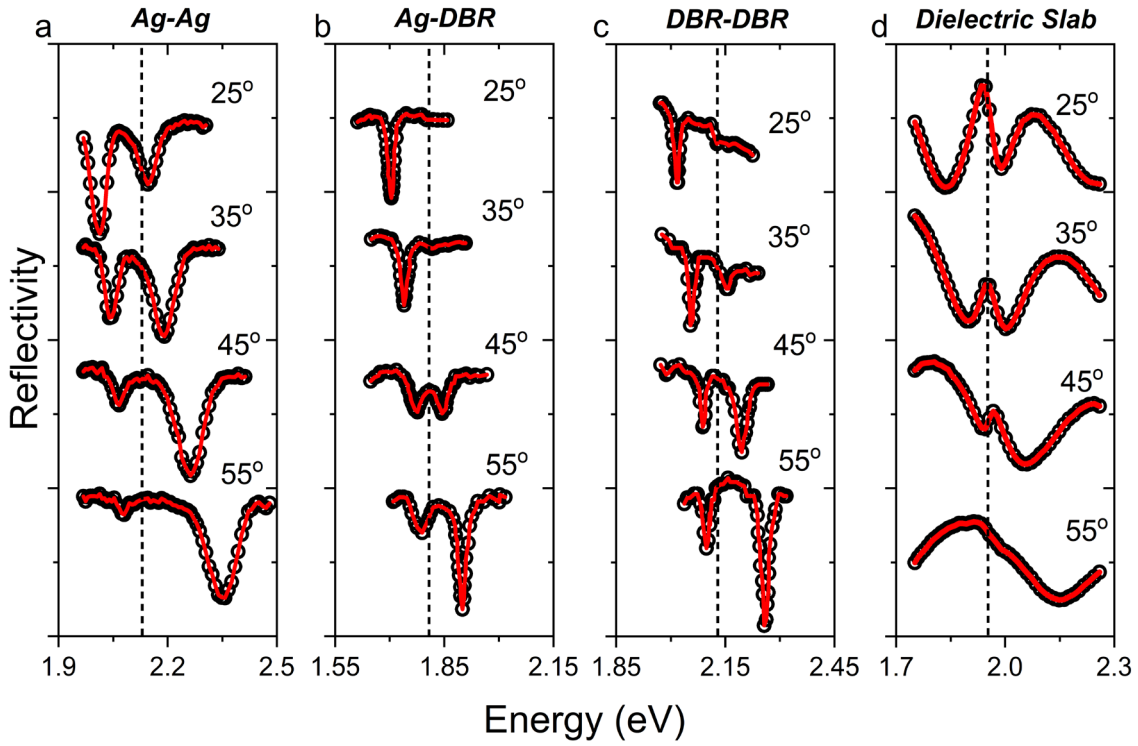

Figure S3. White-light reflectivity data recorded at a series of different angles. Data shown for (a) a metallic Ag-Ag microcavity, (b) a hybrid metallic-dielectric mirror microcavity utilising Ag and DBR mirrors, (c) a double DBR microcavity and (d) a dielectric slab microcavity. Here, data in (a)-(c) has been taken from a selection of our past papers. In each case, the vertical dashed lines represent the energy of the (different) strongly-coupled J-aggregate dye placed in the cavities.

5. TMR modelling for different SiO_2 / organic layer thicknesses

Experiment 1: We have performed a series of TMR simulations in which the thickness of the organic layer was varied at the expense of SiO_2. Here, the *relative concentration of molecules within the active layer was held constant*, but with the total number of molecules increasing as the thickness of the organic layer increases (see Schematic S1). In Figure S4 below it can be seen that the Rabi splitting energy is linearly dependent on the square root of the organic layer thickness *d* (or total number of molecules)[5] with the final point in the plot corresponding to a pure organic film of d = 2550 nm deposited on a high index Nb_2O_5 layer (i.e. with no intermediate SiO_2 layer present).

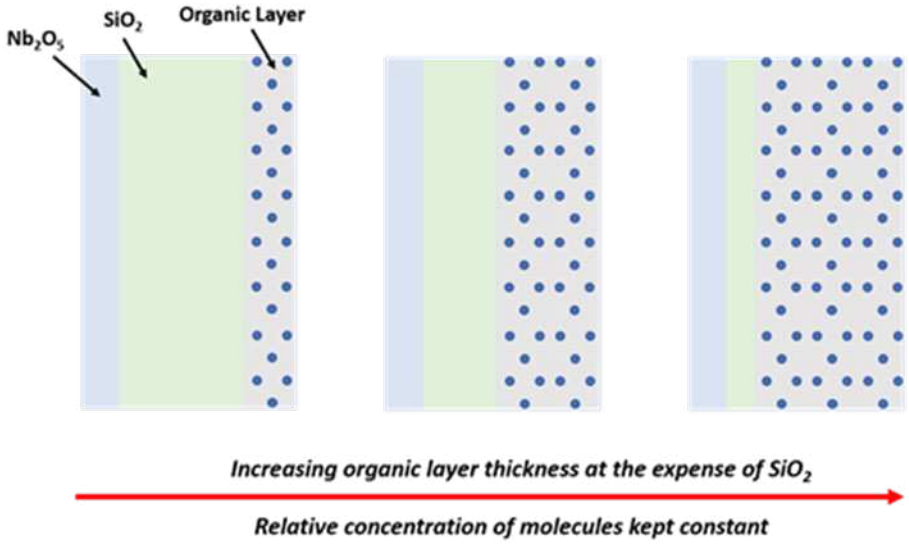

Schematic S1. Dielectric slab resonators in which the thickness of the organic layer was varied at the expense of SiO_2. The relative concentration of molecules within the active layer was held constant, but with the total number of molecules increasing as the thickness of the organic layer increases.

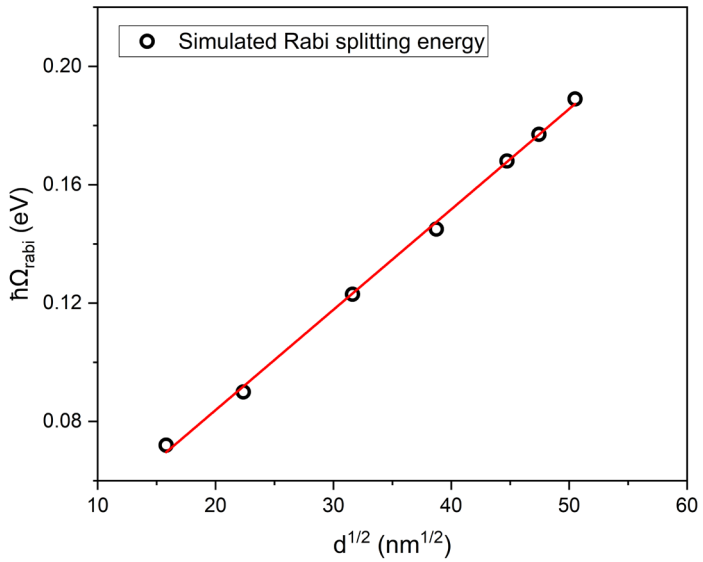

Figure S4. Simulated Rabi splitting energy as a function of the square root of the organic layer thickness, $d^{1/2}$. The thickness of the organic dye layer (d) was varied at the expense of the SiO_2 layer thickness. The red line is a linear fit to the data.

Experiment 2: We have also performed a series of TMR simulations in which the thickness of the organic layer was again varied at the expense of SiO_2. *Here however, the number of molecules within the organic layer was held constant,* with the relative concentration of molecules reducing as the thickness of the organic layer increases (see Schematic S2). Figure S5 shows results of such simulations. Here it can be seen that the Rabi splitting energy varies periodically as a function of organic-semiconductor layer thickness. We believe that this effect results from (i) the overlap of the organic excitons with the periodically varying electric field distribution and (ii) a shift of the energy of the confined optical modes due to changes in the effective refractive index of the cavity with changing organic layer thickness (i.e. different order modes become resonant with the excitons in the angular range probed by the simulations). We mark the mode order next to each group of points in Figure S5.

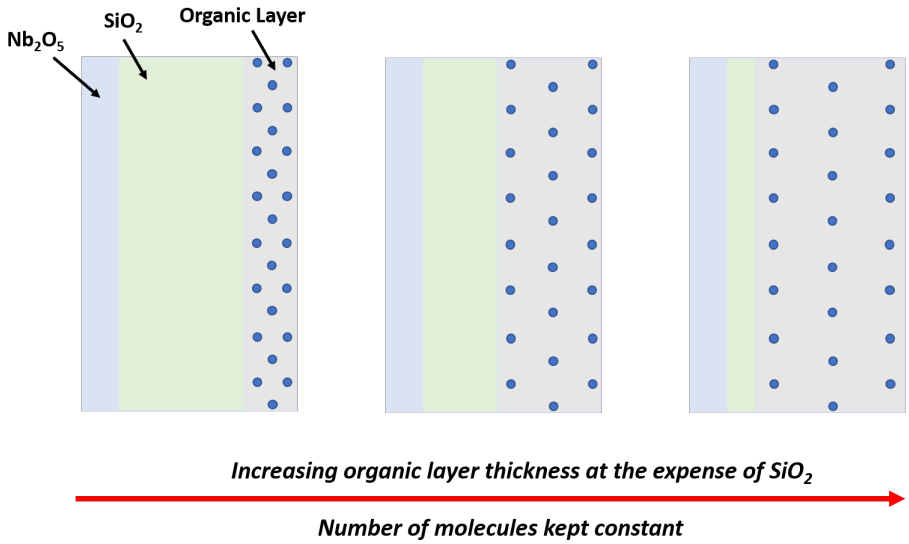

Schematic S2. Dielectric slab resonators in which the thickness of the organic layer was varied at the expense of SiO_2. The number of molecules within the organic layer was held constant, with the relative concentration of molecules reducing as the thickness of the organic layer increases.

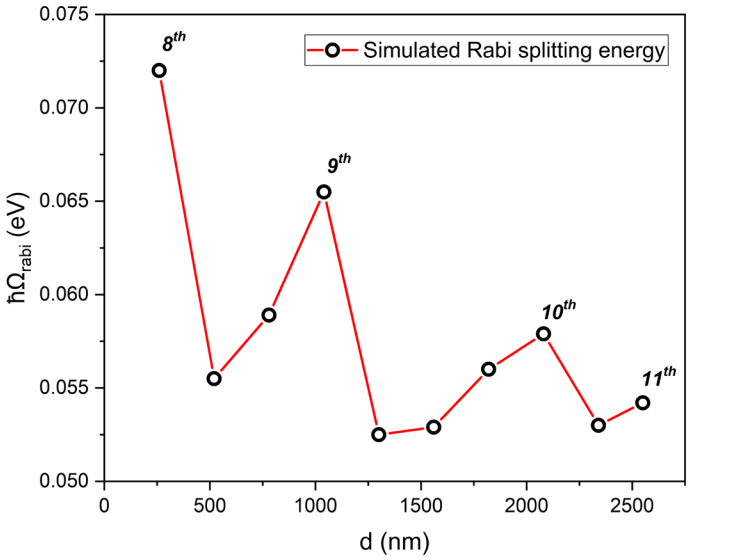

Figure S5. Simulated Rabi splitting energy. Here the thickness of the organic dye (d) was varied at the expense of SiO_2 while keeping the overall number of molecules in the organic layer constant. This results in a reduced concentration of molecules as the thickness of the organic layer (d) increases. The mode order is marked next to each group of points.

Experiment 3: We have performed a series of TMR simulations in which the thickness of the organic layer was kept constant. Here however, we have concentrated all the molecules (total oscillator strength) within a thin (30 nm) organic layer strip that was then placed at different positions along the cavity axis within the organic layer (see Schematic S3). Figure S6 shows results of such simulations where we plot the calculated Rabi splitting energy together with the distribution of the electric field taken from Figure 1b. Here it can be seen that the Rabi splitting energy follows as expected the amplitude of the local electric field.

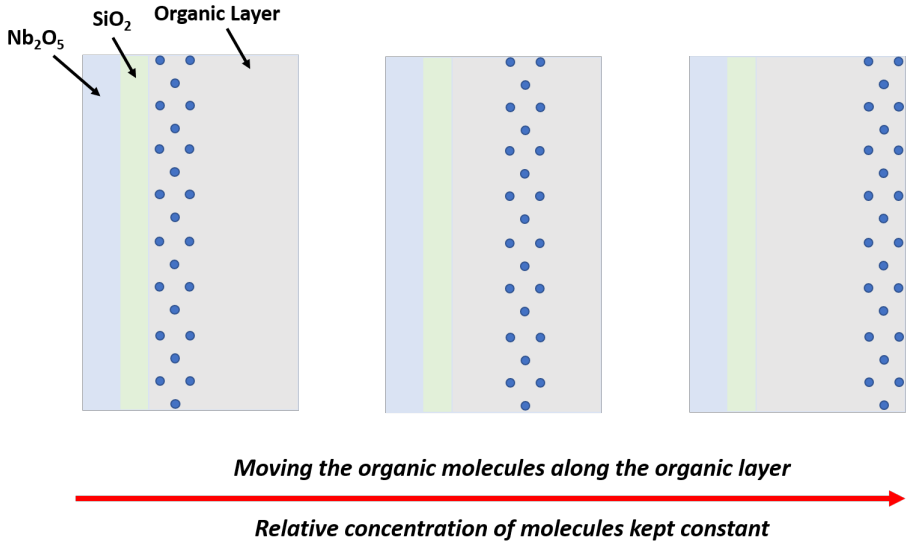

Schematic S3. Dielectric slab resonators in which the thickness of the organic layer was kept constant while the molecules were concentrated in a thin (30 nm) organic layer stripe which was placed at different positions along the organic layer.

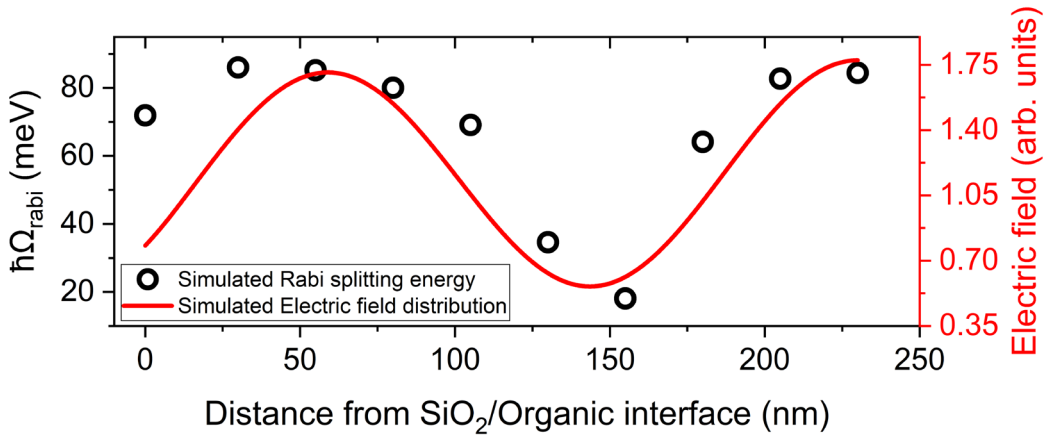

Figure S6. Simulated Rabi splitting energy together with the electric field distribution. Here the thickness of the organic layer was kept constant while the molecules were concentrated in a thin (30 nm) organic layer stripe which was placed at different positions along the organic layer. Open circles plot the Rabi splitting energy, with the red line being the electric field as a function of position within the organic layer (note d = 0 corresponds to the SiO_2/organic interface and d = 225 nm being the organic layer/air interface.

Experiment 4: Here we have simulated the effect of fixing the thickness and oscillator strength of the organic layer, but change the thickness of the SiO_2 dielectric layer (see Schematic 4). The results of the simulations are shown in Figure S7. Note that the Rabi-splitting occurs with different optical modes in the multimode structure as the thickness is varied. Indeed, by reducing the SiO_2 thickness, coupling occurs with lower order modes (corresponding to a reduced cavity length) that have an increased linewidth. In an optical cavity, loss occurs when photons are reflected from the two ends of the active layer (two "mirrors"). Therefore, since the Q-factor is proportional to the lifetime of the photon inside the cavity, a longer cavity length results in a longer photon roundtrip propagation time and consequently a higher Q-factor (narrower cavity linewidth)[6]. For completeness, we plot the simulated HWHM linewidth of the cavity mode as a function of the SiO_2 layer thickness in Figure S7. It can be seen that the Rabi splitting increases as the SiO_2 layer reduces, reaching a maximum value when then SiO_2 layer is around 100 nm. For smaller SiO_2 thickness it then reduces and transits to the weak coupling regime (blue dashed line).

We attribute the observed increase of the Rabi splitting energy with reduced SiO_2 layer thickness (from 2300 nm to 100 nm) to two effects:

1. The reduction of the SiO_2 layer thickness results in a reduced cavity mode volume. Here, keeping the molecular-concentration and thickness of the organic layer fixed while reducing the thickness of SiO_2 layer results in a higher interaction potential and subsequently a larger Rabi splitting energy.

2. According to Savona *et al.*[7], when the cavity mode linewidth becomes comparable to the Rabi-splitting in low-Q factor cavities, it is expected that the Rabi splitting energy increases with increasing cavity mode linewidth[7]. As can be seen in Figure S7, the photon-mode linewidth is a strong function of SiO_2 layer thickness (increasing at reduced thicknesses), and thus this effect also results in an increase in Rabi-splitting energy as the SiO_2 layer thickness is reduced.

However, when the SiO_2 layer approaches a value of 100 nm, the condition for strong coupling defined by Savona *et al.* is only just met[7] due to the relatively broad cavity linewidth. We find that by further reducing the thickness of the SiO_2 dielectric layer below 100 nm results in a sudden reduction of the Rabi splitting energy and a transition to the weak coupling regime[7]. On the figure, we mark the approximate point at which the structure transitions to the weak coupling regime with a blue dashed line.

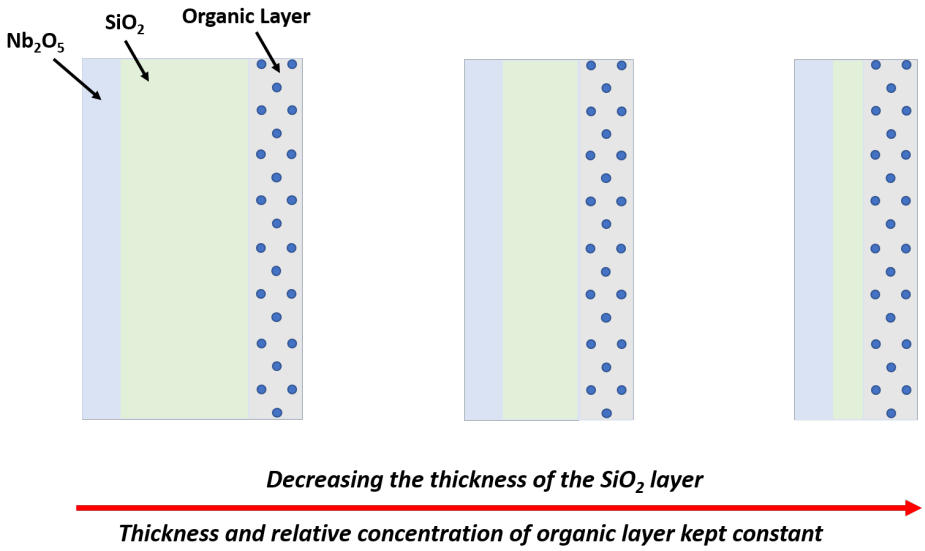

Schematic S4. Dielectric slab resonators in which the thickness and concentration of the organic layer was kept constant while reducing the thickness of the dielectric SiO_2 layer.

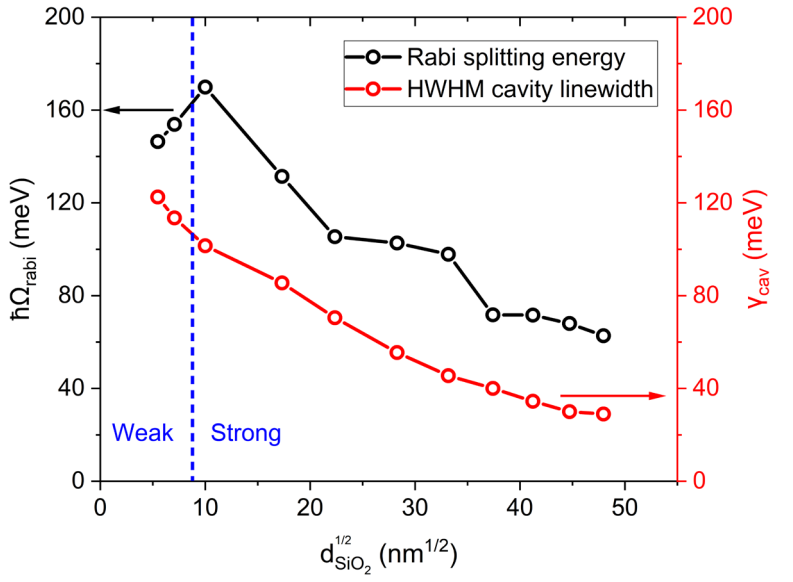

Figure S7. Simulated Rabi splitting energy (black) and HWHM cavity linewidth (red) as a function of SiO_2 thickness. Here the concentration of molecules in the organic layer was kept fixed, with the layer thickness fixed at 250 nm. The blue dashed line indicates approximately the point at which the system transitions to the weak coupling regime (SiO_2 layer thickness below 100 nm).

6. Cross section of reflectivity maps in MTPP microcavities

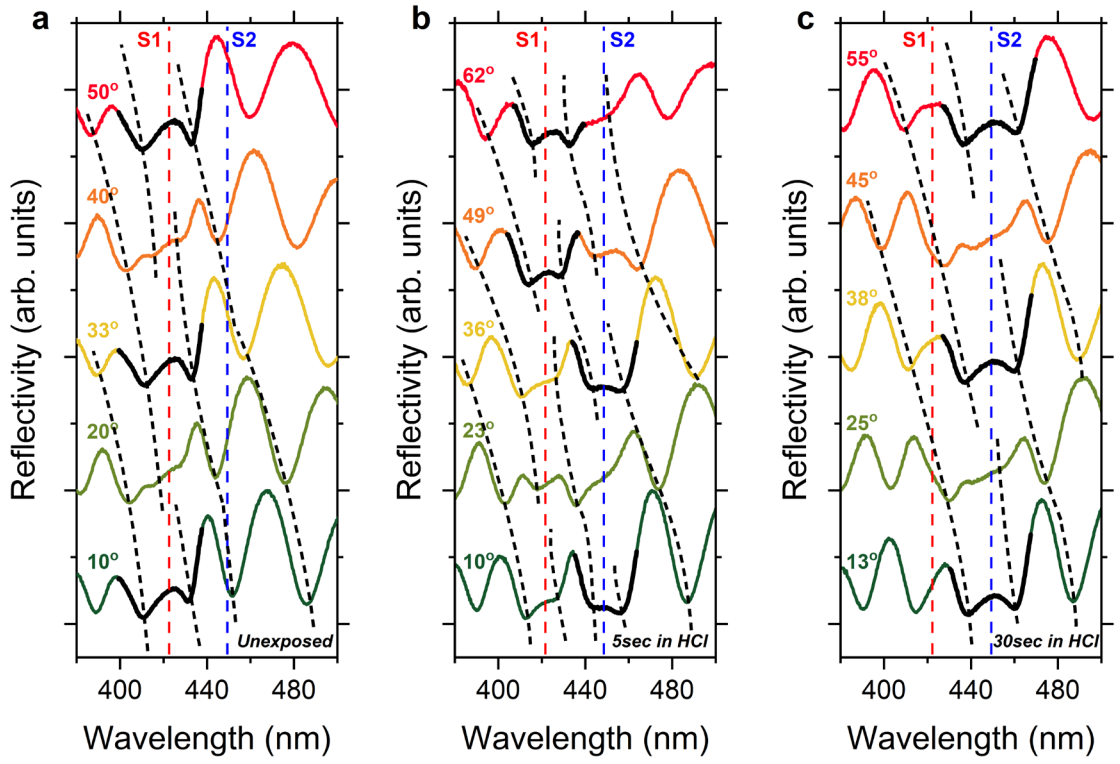

Figure S8. Angle-resolved cross sections of reflectivity maps. This plots the measured white light reflectivity at five individual angles for a microcavity consisting of 150 / 1700 / 225 nm thick layers of Nb_2O_5 / SiO_2 / MTPP when (a) unexposed and when exposed to HCl gas for (b) 5 seconds and (c), 30 seconds. The red and blue dashed lines mark the wavelength of the two different Soret-band excitons (S1 and S2) at 421 nm and 447 nm respectively. The black dashed lines are guides to the eye following the polariton dispersion and the black solid lines mark the energy splitting close to resonance.

7. Strong coupling in water

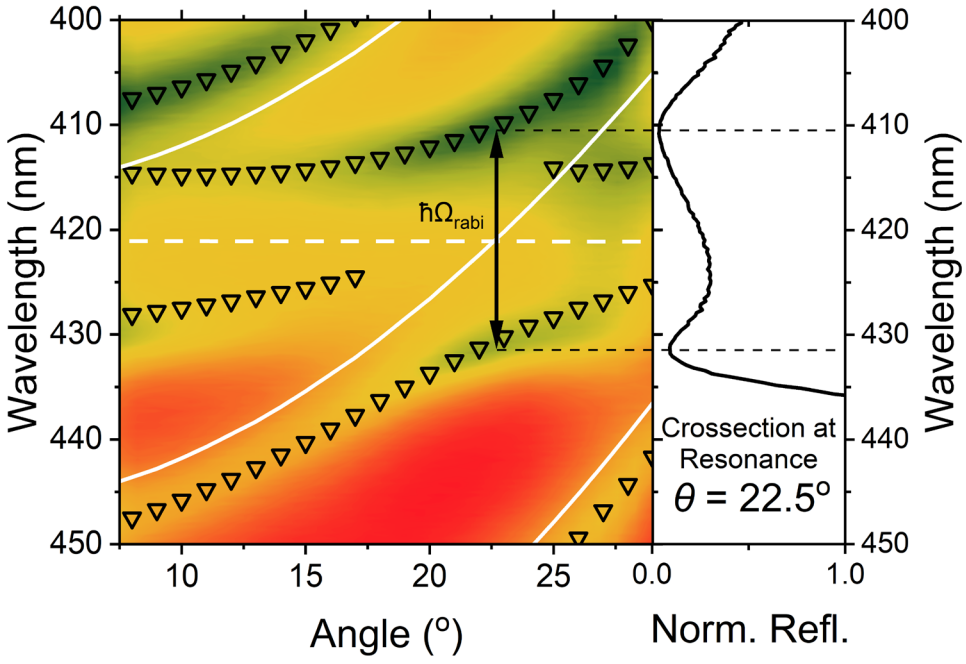

Figure S9. Angle-resolved white reflectivity measurement of a resonator coated with MTPP / PS when fully immersed in water. The goniometer arms were tuned between 10° to 40° in air; an angular range that corresponds to angles between 7.5° and 29° in an aqueous environment. Using a TMR model we mark the exciton energy with a white dashed line, the uncoupled optical modes with white solid lines and the polariton modes with open triangles. The black arrow indicates the Rabi splitting energy ($\hbar\Omega_{rabi}$) resulting from strong exciton-photon coupling. In the right panel we show a cross section of the reflectivity map at the angle of resonance θ=22.5°.

8. Simulated vibrational strong coupling

We have used typical oscillator strength values of vibrational modes in our transfer matrix model to see if such structures can support vibrational strong coupling (VSC). The structure assumed was deposited on a CaF_2 substrate and consisted of 300 nm thick layer of ZnSe followed by a 7000 nm slab of CaF_2. The low-high refractive index value combination of the two layers allowed optical confinement to be achieved. Figure S10 shows TMR simulations of VSC by such a structure when coated with 2000 nm of the polymer PMMA. The confined IR modes strongly couple to the C = O bond resonance of PMMA molecules at ~5773.7nm (shown using a white dashed line)[8,9].

In Table S2 we summarise the values of the HWHM linewidth of the cavity mode and the C = O vibrational mode of PMMA as well as the interaction potential (g) extracted from our coupled oscillator model. Using these values in equation S1 we show that our structure meets the condition for strong coupling[7].

$$g^2 > (\gamma_{cav}^2 + \gamma_{ex}^2)/2 \qquad \text{(S1)}$$

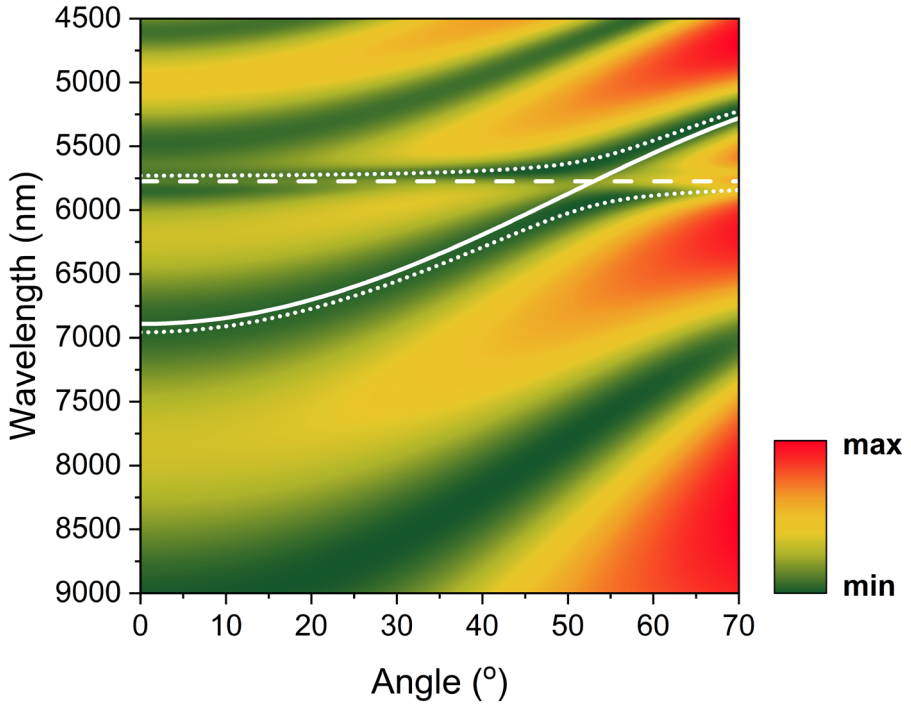

Figure S10. Angular TMR simulations of a multilayer slab structure consisting of ZnSe / CaF_2 / PMMA layers. Here, the relative thicknesses of the layers was 300 nm / 7000 nm / 2000 nm respectively. The wavelength of the C = O bond resonance of PMMA molecules is indicated using a horizontal dashed white line at 5773.7nm (corresponding to a wavenumber of 1732 cm^{-1}). The dotted white line marks the energy of the two polariton modes calculated using a coupled oscillator model. The white solid line represents the energy of the cavity mode.

	Cavity Linewidth γ_{cav} meV	Exciton Linewidth γ_{ex} meV	Interaction Potential g meV	Extinction Coefficient
C = O VSC	**10.75**	**2.3**	**8**	**0.4209**

Table S2. Cavity and exciton HWHM linewidth, Rabi splitting energy and extinction coefficient values used in our coupled oscillator model describing VSC of the PMMA C = O bond resonance to an IR optical mode.

9. References

(1) Furman, S. A.; Tikhonravov, A. V. Spectral Characteristics of Multi-Layer Coatings: Theory. In *Basics of Optics of Multilayer Systems*; 1992; pp 1–102.

(2) Coles, D. M.; Grant, R. T.; Lidzey, D. G.; Clark, C.; Lagoudakis, P. G. Imaging the Polariton Relaxation Bottleneck in Strongly Coupled Organic Semiconductor Microcavities. *Phys. Rev. B* **2013**, *88* (12), 121303.

(3) Lidzey, D. G.; Bradley, D. D. C.; Virgili, T.; Armitage, A.; Skolnick, M. S.; Walker, S. Room Temperature Polariton Emission from Strongly Coupled Organic Semiconductor Microcavities. *Phys. Rev. Lett.* **1999**, *82* (16), 3316–3319.

(4) Coles, D. M.; Michetti, P.; Clark, C.; Tsoi, W. C.; Adawi, A. M.; Kim, J. S.; Lidzey, D. G. Vibrationally Assisted Polariton-Relaxation Processes in Strongly Coupled Organic-Semiconductor Microcavities. *Adv. Funct. Mater.* **2011**, *21* (19), 3691–3696.

(5) D. G. Lidzey; Bradley, D. D. C.; Skolnick, M. S.; Virgili, T.; Walker, S.; Whittaker, D. M. Strong Exciton-Photon Coupling in an Organic Semiconductor Microcavity. *Lett. to Nat.* **1998**, *395*, 53–55.

(6) Kavokin, A. V.; Baumberg, J. J.; Malpuech, G.; Laussy, F. P. *Microcavities*; Oxford Univ. Press, 2007.

(7) Savona, V.; Andreani, L. C.; Schwendimann, P.; Quattropani, A. Quantum Well Excitons in Semiconductor Microcavities: Unified Treatment of Weak and Strong Coupling Regimes. *Solid State Commun.* **1995**, *93* (9), 733–739.

(8) Long, J. P.; Simpkins, B. S. Coherent Coupling between a Molecular Vibration and Fabry-Perot Optical Cavity to Give Hybridized States in the Strong Coupling Limit. *ACS Photonics* **2015**, *2* (1), 130–136.

(9) Menghrajani, K. S.; Nash, G. R.; Barnes, W. L. Vibrational Strong Coupling with Surface Plasmons and the Presence of Surface Plasmon Stop Bands. *ACS Photonics* **2019**, *6* (8), 2110–2116.